https://doi.org/10.1130/G51919.1

Manuscript received 28 November 2023 Revised manuscript received 8 February 2024 Manuscript accepted 21 February 2024

Published online 1 March 2024

© 2024 Geological Society of America. For permission to copy, contact editing@geosociety.org

Strong seismic anisotropy due to upwelling flow at the root of the Yellowstone mantle plume

Jonathan Wolf^{1,*}, Mingming Li², Anne A. Haws¹, and Maureen D. Long¹

¹Department of Earth and Planetary Sciences, Yale University, New Haven 06511, Connecticut, USA ²School of Earth and Space Exploration, Arizona State University, Tempe, Arizona 85281, USA

ABSTRACT

The Yellowstone region (western United States) is a commonly cited example of intraplate volcanism whose origin has been a topic of debate for several decades. Recent work has suggested that a deep mantle plume, rooted beneath southern California, is the source of Yellowstone volcanism. Seismic anisotropy, which typically results from deformation, can be used to identify and characterize mantle flow. Here, we show that the proposed plume root location at the base of the mantle is strongly seismically anisotropic. This finding is complemented by geodynamic modeling results showing upwelling flow and high strains in the lowermost mantle beneath the Yellowstone region. Our results support the idea that the Yellowstone volcanism is caused by a plume rooted in the deepest mantle beneath southern California, connecting dynamics in the deepest mantle with phenomena at Earth's surface.

INTRODUCTION

Mantle plumes, narrow upwellings in Earth's mantle, transport heat to the surface and cause decompression melting and volcanism (e.g., Koppers et al., 2021). While the interactions among plumes and other deep Earth structures are still debated (e.g., Wolf and Evans, 2022; Steinberger and Steinberger, 2023), it is now widely accepted that some plumes originate at the core-mantle boundary region (e.g., French and Romanowicz, 2014; Koppers et al., 2021). Not all intraplate volcanism, however, must be explained by a plume with a deep mantle source (e.g., Long et al., 2012; Fouch, 2012). For example, an upper mantle source has been proposed for the Yellowstone hotspot (western United States) (e.g., Leeman et al., 2009), which may potentially be connected to slab-controlled upwelling (e.g., Faccenna et al., 2010). Recent high-resolution seismic tomography, however, has suggested that Yellowstone volcanism results from a plume rooted in the deepest mantle (Nelson and Grand, 2018).

Plume-associated upwelling flow in the D'' layer should lead to mantle deformation, which in turn may induce the alignment of individual

Jonathan Wolf **b** https://orcid.org/0000-0002 -5440-3791

crystal lattices in a preferred orientation. This alignment causes seismic wave speed through the material to depend on the polarization and/ or propagation direction of the wave, observable via measurements of seismic anisotropy (e.g., Karato et al., 2008). Therefore, seismic anisotropy, which is often studied using shearwave splitting, is an indicator of deformation in the deep mantle (e.g., Romanowicz and Wenk, 2017). D'' anisotropy caused by deformation at plume roots is challenging to measure due to the limited size of the deformed regions and commonly sparse ray coverage. Despite these challenges, seismic anisotropy has previously been associated with the Afar (eastern Africa) (e.g., Ford et al., 2015) and Iceland (Wolf et al., 2019) plumes.

Multiple studies have found D" anisotropy in the general vicinity of the previously suggested Yellowstone plume root (e.g., Long, 2009; Nowacki et al., 2010; Lutz et al., 2020; Asplet et al., 2023). In some of these studies, however, seismic waves did not sample the exact location (e.g., Long, 2009), and in other studies, the methods were not precise enough to pinpoint the D" anisotropy position (e.g., Lutz et al., 2020). This issue pertains especially to the SKS-SKKS differential splitting method, which exploits the fact that SKS and SKKS raypaths in the upper mantle are almost identical,

while they diverge spatially in the lowermost mantle (Fig. 1); therefore, strongly discrepant SKS-SKKS measurements reflect a contribution from D" anisotropy, although a contribution from elsewhere in the lower mantle cannot be completely ruled out (e.g., Tesoniero et al., 2020; Sieminski et al., 2008). The exact location of D" anisotropy, however, is frequently hard to determine using this method. Here we overcome this challenge by examining backazimuthal variations in splitting intensity patterns. We show that SKKS phases, in contrast to SKS, are strongly split due to deep mantle anisotropy close to the location of the Yellowstone plume root suggested by Nelson and Grand (2018). Through geodynamic modeling experiments, we predict strong upwelling flow and large strains in this location. Therefore, convective flow and deformation at the Yellowstone plume root presumably induce the seismic anisotropy we observe, supporting the idea that Yellowstone volcanism originates from a plume formed at the core-mantle boundary.

SHEAR-WAVE SPLITTING MEASUREMENTS

Analogous to optical birefringence, shear waves that travel through an anisotropic material split into fast and slow components (e.g., Silver and Chan, 1991). Measurable shear-wave splitting parameters include the time lag between these two components (δt) and the polarization direction of the fast-traveling wave (ϕ). Splitting intensity (SI) (Chevrot, 2000), a quantity that indicates splitting strength on an individual seismogram, is expressed as:

$$SI \approx \delta t \sin[2(b - \varphi)],$$
 (1)

where *b* is the backazimuth for SKS and SKKS waves. We use SplitRacer_auto software (Link et al., 2022) to measure splitting parameters, bandpass filtering our data between 6 and 25 s

CITATION: Wolf, J., et al., 2024, Strong seismic anisotropy due to upwelling flow at the root of the Yellowstone mantle plume: Geology, v. 52, p. 379–382, https://doi.org/10.1130/G51919.1

^{*}jonathan.wolf@yale.edu

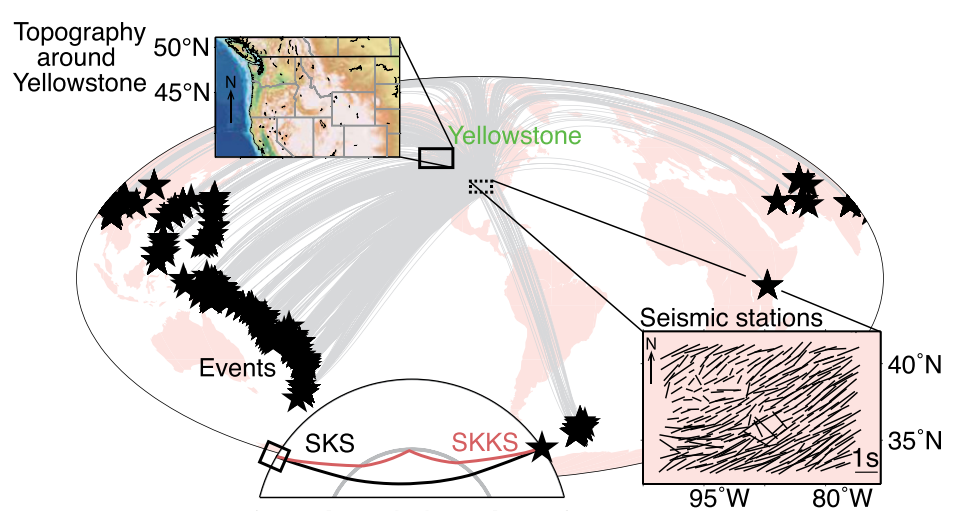
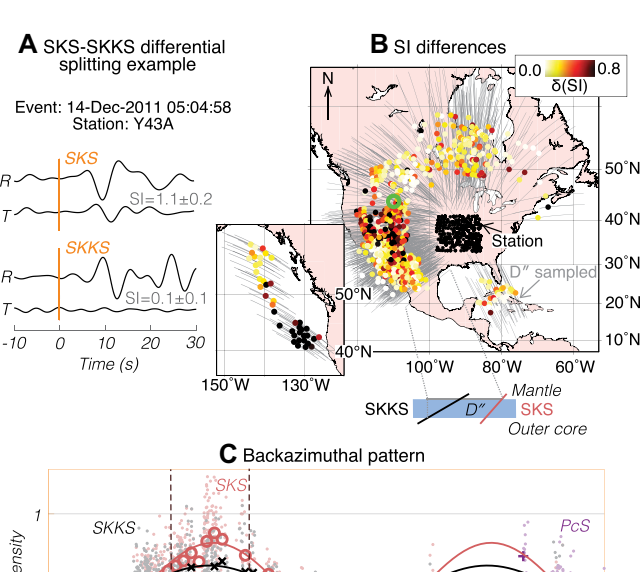


Figure 1. Great-circle raypaths (gray lines) from source (black star) to station region (black dashed rectangle). Yellowstone hotspot surface location is shown as green circle. Inset at bottom left: Cross-section of SKS (black) and SKKS (red) raypaths for an epicentral distance of 115°. Surface (black) and core-mantle boundary (gray) are represented as semicircles. Inset at top left: Topography map around Yellowstone. Right inset: Previously reported single-station average splitting measurements (φ , δt [see text]) for seismic stations we use (Link et al., 2022).

before conducting the analysis. We define SKS-SKKS differential splitting measurements as well constrained if the waveforms have signal-to-noise ratios >2.5 for both phases and SI 95% uncertainty intervals < \pm 0.4.

SEISMIC DATA AND RESULTS

For our splitting analysis, we use all available broadband seismic stations between latitudes 33°N and 41°N and longitudes 98°W and 83°W (Fig. 1) and seismic events with moment



SKKS D" SKS
Outer core

C Backazimuthal pattern

SKS

Outer core

Assumption of the content of t

Figure 2. Differential SKS-SKKS splitting results. (A) Example SKS and SKKS radial (R) and transverse (T) seismograms recorded at station Y43A. Predicted arrival times for Preliminary Reference Earth Model (Dziewonski and Anderson, 1981) are shown as vertical orange lines. SKKS splitting is null (splitting intensity, SI = 0.1), while SKS is strongly split (SI = 1.1). (B) SI differences for whole data set. Stations (black circles), D" portion sampled by SKS and SKKS (gray lines), and SI discrepancies are shown (colored dots in the middle of the gray lines; see legend). Green circle shows surface location of Yellowstone hotspot. Inset: SKS-SKKS SI discrepancies previously obtained by Wolf et al. (2023a) for an event on 5 September 2011 at a different set of stations. (C)

SKS (red dots) and SKKS (black dots) SI values as function of backazimuth (defined clockwise from north), and binned averages (bin width: 7° ; SKS, red circles; SKKS, black crosses). Splitting is discrepant between backazimuths -100° and -50° . Fitted $\sin[2(b-\varphi)]$ curves (b= backazimuth; $\varphi=$ polarization direction) are presented as black (SKKS) and red (SKS) lines. Violet dots represent individual PcS splitting measurements (D. Frost, 2023, personal commun.), with plus signs indicating backazimuthal bins.

magnitudes >5.8 that occurred after 1 January 1990. SKS and SKKS phases recorded in this region sample D" close to the Yellowstone plume root location suggested by Nelson and Grand (2018). Wolf et al. (2023a) found evidence for differential SKS-SKKS splitting using splitting measurements from data stacked across subarrays of the USArray seismograph network (IRIS Transportable Array, 2003) in this region. However, measurements using the time-limited USArray data were too sparse to pinpoint the exact location of deep mantle anisotropy. Here we use a complementary approach, with a larger number of single-station splitting measurements for a longer time period, essentially compromising signal clarity for data quantity. Figure 1 shows all events for which well-constrained SKS-SKKS differential SI measurements were obtained as well as previous upper mantle splitting results for our station region. Differential SKS-SKKS splitting results are presented in Figure 2. Figure 2A shows an example for a differentially split SKS-SKKS pair recorded at station Y43A. For this example, SKKS splitting is null, while SKS is clearly split, with SI = 1.1. All differential SI values, projected to the D'' region, are displayed in Figure 2B. For most of the backazimuthal swath, differential SI values are <0.4, indicating little or no contribution from the deep mantle. However, for SKS and SKKS waves arriving from backazimuths between -100° and -50° , SKS-SKKS splitting is strongly discrepant, indicating that one or both phases are influenced by lowermost mantle anisotropy. The region in which we find discrepant SKS-SKKS splitting is in the vicinity of where Wolf et al. (2023a) also found differential SI values using stacked data (Fig. 2B inset).

LOCATING LOWERMOST MANTLE ANISOTROPY

It is not possible to determine whether SKS, SKKS, or both phases are influenced by D''anisotropy using individual SKS-SKKS differential splitting measurements (Wolf et al., 2022). In an idealized case with perfect backazimuthal coverage at a single station with (laterally homogeneous and horizontal) anisotropic layers beneath it, SI values would be distributed along a curve proportional to $\sin[2(b-\phi)]$ (see Equation 1). The argument that upper mantle anisotropy can be approximated as a laterally homogeneous and horizontal layer (in certain cases) allows us to determine which seismic phase(s) is influenced by lowermost mantle anisotropy. In our case (Fig. 2C), the backazimuthally binned SI values for SKS almost perfectly fit a $\sin[2(b - \phi)]$ curve; in contrast, SKKS deviates significantly from this pattern between backazimuths -100° and -50° . This is the backazimuthal interval across which we observe SKS-SKKS SI discrepancies; otherwise, splitting is nondiscrepant. As an addi-

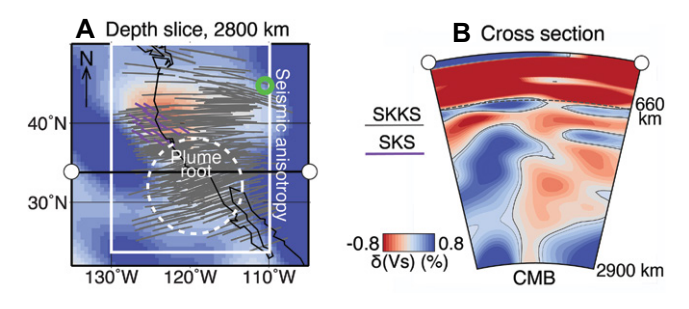


Figure 3. Seismological and geodynamic modeling results. (A) SKS (from Wolf et al., 2023a; violet lines) and SKKS (this study, gray lines) raypaths that sample the inferred region of D" anisotropy. Background colors indicate velocity perturbations at 2800 km depth according to S40RTS seismic tomography model

(Ritsema et al., 2011; see legend). White box indicates approximate location of D" anisotropy, and dashed circle, the deep mantle location of Yellowstone plume suggested by Nelson and Grand (2018). Green circle represents surface location of Yellowstone hotspot. Low-velocity location in S40RTS is slightly north of the plume root location suggested by Nelson and Grand (2018). (B) Cross section through S40RTS along profile indicated by solid white circles in A. Nearly vertically continuous low-velocity structure indicates the upwelling plume. CMB—coremantle boundary.

tional constraint on upper mantle anisotropy in our study region, we also show PcS beam splitting measurements (D. Frost, 2023, personal commun.) in Figure 2C. The $\sin[2(b-\phi)]$ fit for SKS also matches these PcS SI values well, again in contrast to that of SKKS, which shows a significant deviation. We therefore infer that while SKS, SKKS, and PcS all sample similar upper mantle anisotropy, SKKS also samples D'' anisotropy in the backazimuthal swath between -100° and -50° , leading to lower SKKS SI values that deviate from the upper mantle anisotropy curve.

This argument is supported by another, independent line of evidence: Wolf et al. (2023a) detected discrepant SKS-SKKS splitting using stacked data pairs that sample D" beneath the U.S. west coast or the eastern Pacific Ocean (Fig. 2B inset). For those pairs, the SKS waves sample D" in the same location as the SKKS phases that are analyzed in this work (Fig. 3A).

Α

3 cm/yr

140°W

-0.4 -0.2 0.0 0.2 0.4

Radial velocity (cm/yr)

The measurements by Wolf et al. (2023a) are likely discrepant because SKS samples D" anisotropy in this region, which influences SKKS phases in this study. (Note that the SKKS raypaths through D", displayed in Fig. 3A, lie to the west of the SKS-SKKS midpoints in D" used to display SI differences in Fig. 2B). Our results (Fig. 2C) also indicate regions of null (or weak) splitting due to D'' anisotropy for backazimuths at which SKS-SKKS splitting is nondiscrepant. Due to a lack of ray coverage, our study region is not well suited for obtaining additional constraints using other commonly used seismic phases to determine D" anisotropy, such as ScS and Sdiff. Additionally, while SKS-SKKS differential splitting is a reliable indicator of seismic anisotropy in the lowermost mantle, well-constrained fast polarization directions and delay times are challenging to obtain, particularly for (frequently noisy) single-station measurements. Therefore, it is not possible to infer

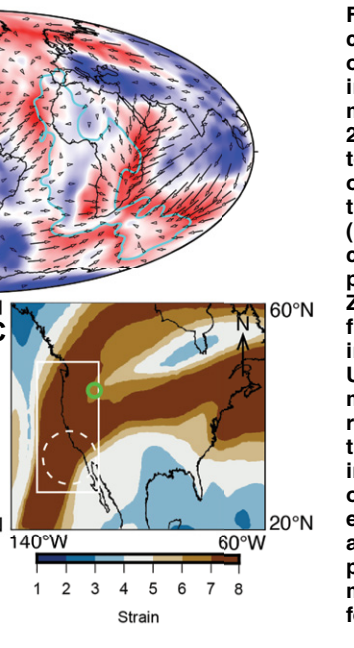


Figure 4. Geodynamically derived distribution of mantle flow and strain in D" layer. (A) Global mantle flow field at 2800 km depth. Cyan contours show Vs anomaly of -0.5% in the S40RTS tomography model (Ritsema et al., 2011), indicating large low-velocity province regions. (B) Zoom-in of mantle flow field marked by red box in panel A beneath the United States. (C) Accumulated strain in same region as in B. Other plotting conventions are as in Figure 3A. Results for other models with different model parameters and model setup are presented in the Supplemental Material (see text footnote 1).

flow directions via forward or inverse modeling approaches, as in some previous D" anisotropy studies (e.g., Wolf and Long, 2022; Asplet et al., 2023). Instead, we choose an approach that compares shear-wave splitting results to deformation and strain patterns inferred using geodynamic modeling.

MANTLE FLOW AND DEFORMATION IN THE STUDY REGION

High-resolution tomography models consistently show relatively low shear-wave velocities where we observe deep mantle anisotropy (e.g., Ritsema et al., 2011; French and Romanowicz, 2014; Nelson and Grand, 2018), indicating higher mantle temperatures than in the surroundings. Nelson and Grand (2018) suggested that these low velocities correspond to the root of the Yellowstone plume, which reaches the surface to the northeast of its deep mantle source region (Fig. 3). When deformation is accommodated by dislocation creep, strain causes the alignment of individual mineral crystals, which can result in seismic anisotropy, as measured by shear-wave splitting. We conduct geodynamic simulations to investigate the mantle flow field and deformation in the lowermost mantle beneath Yellowstone. We calculate the present-day instantaneous global mantle flow field by solving the conservation equations of mass and momentum using a density field derived from seismic tomography model S40RTS (Ritsema et al., 2011). Using this mantle flow field, we derive strain, which is a measure of deformation. The details of geodynamic simulations are presented in the Supplemental Material1.

We find that the lateral mantle flow generally moves from downwelling centers toward the two large low-velocity provinces (LLVPs) and that upwelling occurs mostly in regions within, at, and outside the boundaries of the LLVPs (Fig. 4A). In particular, mantle flow beneath the western United States moves southwestward, which is consistent with the findings of Steinberger et al. (2019). We also find relatively strong upwelling flow in the previously suggested plume root location (Fig. 4B), which corresponds to the region of strong D" anisotropy. These results are robust across different assumptions made in our geodynamic models (Fig. 4B; Figs. S1-S2 [see footnote 1]). We suggest that the change of flow near the base of the Yellowstone plume (Fig. 4B) causes significant deformation, inducing lattice-preferred orientation and therefore seismic anisotropy. The deformation may be linked to convergent lateral flow at the base of the upwelling. To test

60°W

^{&#}x27;Supplemental Material. Supplemental text and equations, Figures S1–S2, and Table S1. Please visit https://doi.org/10.1130/GEOL.S.25263166 to access the supplemental material; contact editing@geosociety.org with any questions.

these hypotheses, we calculate strain from our inferred present-day flow field. We find large strains (>4) in the region where seismic anisotropy is detected (Fig. 4C); this feature appears across different models (Fig. S1). It is possible that the flow within the plume root may also contribute to deformation, but this is not clearly resolvable in our models in which the density structure is derived from global tomography models with limited resolution (Steinberger et al., 2019). Future work that includes a comparison to realistic plume models has potential to shed more light on the mechanism causing seismic anisotropy.

We thus conclude that there is significant D" anisotropy co-located with the deep mantle root of the Yellowstone plume. Our geodynamic models show that this seismic anisotropy is caused by upwelling flow, resulting in a large accumulation of strain. Our results provide additional support for the idea that Yellowstone hotspot volcanism is caused by a deep mantle plume, connecting dynamics in the deepest mantle with phenomena at Earth's surface.

ACKNOWLEDGMENTS

This work was funded by Yale University and the National Science Foundation via grants EAR-2054926 to Li and EAR-2026917 to Long. We used Generic Mapping Tools (Wessel and Smith, 1998) and SubMachine (Hosseini et al., 2018). We thank Poulami Roy, Bernhard Steinberger, and two anonymous reviewers for helpful suggestions. Data sources are acknowledged in the Supplemental Material.

REFERENCES CITED

- Asplet, J., Wookey, J., and Kendall, M., 2023, Inversion of shear wave waveforms reveal deformation in the lowermost mantle: Geophysical Journal International, v. 232, p. 97–114, https://doi.org/10.1093/gji/ggac328.
- Chevrot, S., 2000, Multichannel analysis of shear wave splitting: Journal of Geophysical Research, v. 105, p. 21,579–21,590, https://doi.org/10.1029/2000JB900199.
- Dziewonski, A.M., and Anderson, D.L., 1981, Preliminary reference Earth model: Physics of the Earth and Planetary Interiors, v. 25, p. 297–356, https://doi.org/10.1016/0031-9201(81)90046-7.
- Faccenna, C., Becker, T.W., Lallemand, S., Lagabrielle, Y., Funiciello, F., and Piromallo, C., 2010, Subduction-triggered magmatic pulses: A new class of plumes?: Earth and Planetary Science Letters, v. 299, p. 54–68, https://doi.org/10.1016/j.epsl.2010.08.012.
- Ford, H.A., Long, M.D., He, X., and Lynner, C., 2015, Lowermost mantle flow at the eastern edge of the African Large Low Shear Velocity Province: Earth and Planetary Science Letters, v. 420, p. 12–22, https://doi.org/10.1016/j.epsl.2015.03.029.
- Fouch, M.J., 2012, The Yellowstone hotspot: Plume or not?: Geology, v. 40, p. 479–480, https://doi.org/10.1130/focus052012.1.

- French, S.W., and Romanowicz, B.A., 2014, Wholemantle radially anisotropic shear velocity structure from spectral-element waveform tomography: Geophysical Journal International, v. 199, p. 1303–1327, https://doi.org/10.1093/gij/ggu334.
- Hosseini, K., Matthews, K.J., Sigloch, K., Shephard, G.E., Domeier, M., and Tsekhmistrenko, M., 2018, SubMachine: Web-based tools for exploring seismic tomography and other models of Earth's deep interior: Geochemistry, Geophysics, Geosystems, v. 19, p. 1464–1483, https://doi .org/10.1029/2018GC007431.
- IRIS Transportable Array, 2003, USArray Transportable Array: International Federation of Digital Seismograph Networks, https://doi.org/10.7914/SN/TA (last accessed Feb. 2023).
- Karato, S.-i., Jung, H., Katayama, I., and Skemer, P., 2008, Geodynamic significance of seismic anisotropy of the upper mantle: New insights from laboratory studies: Annual Review of Earth and Planetary Sciences, v. 36, p. 59–95, https://doi .org/10.1146/annurev.earth.36.031207.124120.
- Koppers, A.A.P., Becker, T.W., Jackson, M.G., Konrad, K., Müller, R.D., Romanowicz, B., Steinberger, B., and Whittaker, J.M., 2021, Mantle plumes and their role in Earth processes: Nature Reviews Earth & Environment, v. 2, p. 382–401, https://doi.org/10.1038/s43017-021-00168-6.
- Leeman, W.P., Schutt, D.L., and Hughes, S.S., 2009, Thermal structure beneath the Snake River Plain: Implications for the Yellowstone hotspot: Journal of Volcanology and Geothermal Research, v. 188, p. 57–67, https://doi.org/10.1016/j.jvolgeores.2009.01.034.
- Link, F., Reiss, M.C., and Rümpker, G., 2022, An automatized XKS-splitting procedure for large data sets: Extension package for SplitRacer and application to the USArray: Computers & Geosciences, v. 158, https://doi.org/10.1016/j.cageo .2021.104961.
- Long, M.D., 2009, Complex anisotropy in D" beneath the eastern Pacific from SKS–SKKS splitting discrepancies: Earth and Planetary Science Letters, v. 283, p. 181–189, https://doi.org/10.1016/j.epsl .2009.04.019.
- Long, M.D., Till, C.B., Druken, K.A., Carlson, R.W., Wagner, L.S., Fouch, M.J., James, D.E., Grove, T.L., Schmerr, N., and Kincaid, C., 2012, Mantle dynamics beneath the Pacific Northwest and the generation of voluminous back-arc volcanism: Geochemistry, Geophysics, Geosystems, v. 13, Q0AN01, https://doi.org/10.1029 /2012GC004189.
- Lutz, K.A., Long, M.D., Creasy, N., and Deng, J., 2020, Seismic anisotropy in the lowermost mantle beneath North America from SKS-SKKS splitting intensity discrepancies: Physics of the Earth and Planetary Interiors, v. 305, https://doi.org/10 .1016/j.pepi.2020.106504.
- Nelson, P.L., and Grand, S.P., 2018, Lower-mantle plume beneath the Yellowstone hotspot revealed by core waves: Nature Geoscience, v. 11, p. 280–284, https://doi.org/10.1038/s41561-018-0075-y.
- Nowacki, A., Wookey, J., and Kendall, J.-M., 2010, Deformation of the lowermost mantle from seismic anisotropy: Nature, v. 467, p. 1091–1094, https://doi.org/10.1038/nature09507.
- Ritsema, J., Deuss, A., van Heijst, H.J., and Woodhouse, J.H., 2011, S40RTS: A degree-40 shear-

- velocity model for the mantle from new Rayleigh wave dispersion, teleseismic traveltime and normal-mode splitting function measurements: Geophysical Journal International, v. 184, p. 1223–1236, https://doi.org/10.1111/j.1365-246X.2010 04884 x
- Romanowicz, B., and Wenk, H.-R., 2017, Anisotropy in the deep Earth: Physics of the Earth and Planetary Interiors, v. 269, p. 58–90, https://doi.org/10.1016/j.pepi.2017.05.005.
- Sieminski, A., Paulssen, H., Trampert, J., and Tromp, J., 2008, Finite-frequency SKS splitting: Measurement and sensitivity kernels: Bulletin of the Seismological Society of America, v. 98, p. 1797– 1810, https://doi.org/10.1785/0120070297.
- Silver, P.G., and Chan, W.W., 1991, Shear wave splitting and subcontinental mantle deformation: Journal of Geophysical Research, v. 96, p. 16,429–16,454, https://doi.org/10.1029/91JB00899.
- Steinberger, B., and Steinberger, A., 2023, Mantle plumes and their interactions, in Duarte, J.C., ed., Dynamics of Plate Tectonics and Mantle Convection: Amsterdam, Elsevier, p. 407–426, https:// doi.org/10.1016/B978-0-323-85733-8.00021-4.
- Steinberger, B., Nelson, P.L., Grand, S.P., and Wang, W., 2019, Yellowstone plume conduit tilt caused by large-scale mantle flow: Geochemistry, Geophysics, Geosystems, v. 20, p. 5896–5912, https://doi.org/10.1029/2019GC008490.
- Tesoniero, A., Leng, K., Long, M.D., and Nissen-Meyer, T., 2020, Full wave sensitivity of SK(K) S phases to arbitrary anisotropy in the upper and lower mantle: Geophysical Journal International, v. 222, p. 412–435, https://doi.org/10.1093/gji/ggaa171.
- Wessel, P., and Smith, W.H.F., 1998, New, improved version of Generic Mapping Tools released: Eos (Transactions, American Geophysical Union), v. 79, p. 579, https://doi.org/10.1029/98EO00426.
- Wolf, J., and Evans, D.A.D., 2022, Reconciling supercontinent cycle models with ancient subduction zones: Earth and Planetary Science Letters, v. 578, https://doi.org/10.1016/j.epsl.2021 117293
- Wolf, J., and Long, M.D., 2022, Slab-driven flow at the base of the mantle beneath the northeastern Pacific Ocean: Earth and Planetary Science Letters, v. 594, https://doi.org/10.1016/j.epsl.2022 .117758.
- Wolf, J., Creasy, N., Pisconti, A., Long, M.D., and Thomas, C., 2019, An investigation of seismic anisotropy in the lowermost mantle beneath Iceland: Geophysical Journal International, v. 219, p. S152–S166, https://doi.org/10.1093/gji/ggz312.
- Wolf, J., Long, M.D., Leng, K., and Nissen-Meyer, T., 2022, Constraining deep mantle anisotropy with shear wave splitting measurements: Challenges and new measurement strategies: Geophysical Journal International, v. 230, p. 507–527, https://doi.org/10.1093/gji/ggac055.
- Wolf, J., Frost, D.A., Long, M.D., Garnero, E., Aderoju, A.O., Creasy, N., and Bozdağ, E., 2023, Observations of mantle seismic anisotropy using array techniques: Shear-wave splitting of beamformed SmKS phases: Journal of Geophysical Research: Solid Earth, v. 128, https://doi.org/10.1029/2022JB025556.

Printed in the USA